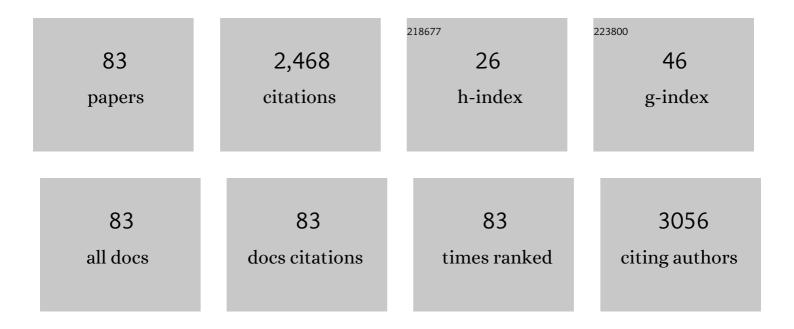
List of Publications by Year in descending order

Source: https://exaly.com/author-pdf/5862909/publications.pdf Version: 2024-02-01



#	Article	IF	CITATIONS
1	Synthesis of nitrogen-doping carbon dots with different photoluminescence properties by controlling the surface states. Nanoscale, 2016, 8, 6770-6776.	5.6	214
2	An inner filter effect based sensor of tetracycline hydrochloride as developed by loading photoluminescent carbon nanodots in the electrospun nanofibers. Nanoscale, 2016, 8, 2999-3007.	5.6	194
3	Highly selective detection of 2,4,6-trinitrophenol by using newly developed terbium-doped blue carbon dots. Analyst, The, 2016, 141, 2676-2681.	3.5	136
4	Inner filter with carbon quantum dots: A selective sensing platform for detection of hematin in human red cells. Biosensors and Bioelectronics, 2018, 100, 148-154.	10.1	96
5	A functional preservation strategy for the production of highly photoluminescent emerald carbon dots for lysosome targeting and lysosomal pH imaging. Nanoscale, 2018, 10, 14705-14711.	5.6	86
6	Photothermal Soft Nanoballs Developed by Loading Plasmonic Cu _{2–<i>x</i>} Se Nanocrystals into Liposomes for Photothermal Immunoassay of Aflatoxin B ₁ . Analytical Chemistry, 2019, 91, 4444-4450.	6.5	84
7	A graphitic carbon nitride based fluorescence resonance energy transfer detection of riboflavin. Talanta, 2016, 148, 279-284.	5.5	72
8	Photoluminescence of carbon quantum dots: coarsely adjusted by quantum confinement effects and finely by surface trap states. Science China Chemistry, 2018, 61, 490-496.	8.2	72
9	Cu(<scp>i</scp>)-Doped carbon quantum dots with zigzag edge structures for highly efficient catalysis of azide–alkyne cycloadditions. Green Chemistry, 2017, 19, 1494-1498.	9.0	65
10	Functional preserving carbon dots-based fluorescent probe for mercury (II) ions sensing in herbal medicines via coordination and electron transfer. Analytica Chimica Acta, 2018, 1035, 203-210.	5.4	60
11	Visually monitoring the etching process of gold nanoparticles by KI/I2 at single-nanoparticle level using scattered-light dark-field microscopic imaging. Nano Research, 2016, 9, 1125-1134.	10.4	58
12	Dendritic CuSe with Hierarchical Side-Branches: Synthesis, Efficient Adsorption, and Enhanced Photocatalytic Activities under Daylight. ACS Sustainable Chemistry and Engineering, 2017, 5, 4154-4160.	6.7	54
13	Carbon dots as nanocatalytic medicine for anti-inflammation therapy. Journal of Colloid and Interface Science, 2022, 611, 545-553.	9.4	49
14	Use of the peroxidase mimetic activity of erythrocyte-like Cu _{1.8} S nanoparticles in the colorimetric determination of glutathione. Analytical Methods, 2017, 9, 841-846.	2.7	46
15	"Click―on Alkynylated Carbon Quantum Dots: An Efficient Surface Functionalization for Specific Biosensing and Bioimaging. Chemistry - A European Journal, 2017, 23, 2171-2178.	3.3	44
16	Radial Basis Function Network-Based Transform for a Nonlinear Support Vector Machine as Optimized by a Particle Swarm Optimization Algorithm with Application to QSAR Studies. Journal of Chemical Information and Modeling, 2007, 47, 1438-1445.	5.4	43
17	Studying the Interaction of Pirarubicin with DNA and Determining Pirarubicin in Human Urine Samples: Combining Excitation -Emission Fluorescence Matrices with Second-order Calibration Methods. Journal of Fluorescence, 2009, 19, 955-966.	2.5	42
18	General Sensitive Detecting Strategy of Ions through Plasmonic Resonance Energy Transfer from Gold Nanoparticles to Rhodamine Spirolactam. Analytical Chemistry, 2017, 89, 1808-1814.	6.5	40

#	Article	IF	CITATIONS
19	Single Plasmonic Nanosprings for Visualizing Reactive-Oxygen-Species-Activated Localized Mechanical Force Transduction in Live Cells. ACS Nano, 2017, 11, 541-548.	14.6	39
20	Real-time monitoring of oxidative etching on single Ag nanocubes via light-scattering dark-field microscopy imaging. Nanoscale, 2015, 7, 15209-15213.	5.6	36
21	Plasmon-induced light concentration enhanced imaging visibility as observed by a composite-field microscopy imaging system. Chemical Science, 2016, 7, 5477-5483.	7.4	35
22	Luminol and gold nanoparticle-co-precipitated reduced graphene oxide hybrids with long-persistent chemiluminescence for cholesterol detection. Journal of Materials Chemistry B, 2017, 5, 7335-7341.	5.8	32
23	Self-Targeting Carbon Quantum Dots for Peroxynitrite Detection and Imaging in Live Cells. Analytical Chemistry, 2021, 93, 16466-16473.	6.5	32
24	Synergetic Catalytic Effect of Cu2–xSe Nanoparticles and Reduced Graphene Oxide Coembedded in Electrospun Nanofibers for the Reduction of a Typical Refractory Organic Compound. ACS Applied Materials & Interfaces, 2015, 7, 15447-15457.	8.0	29
25	Plasmonic Cu _{2–<i>x</i>} S _{<i>y</i>} Se _{1–<i>y</i>} Nanoparticles Catalyzed Click Chemistry Reaction for SERS Immunoassay of Cancer Biomarker. Analytical Chemistry, 2018, 90, 11728-11733.	6.5	28
26	Boosting support vector regression in QSAR studies of bioactivities of chemical compounds. European Journal of Pharmaceutical Sciences, 2006, 28, 344-353.	4.0	27
27	Variable-weighted least-squares support vector machine for multivariate spectral analysis. Talanta, 2010, 80, 1698-1701.	5.5	27
28	Precision improvement in dark-field microscopy imaging by using gold nanoparticles as an internal reference: a combined theoretical and experimental study. Nanoscale, 2016, 8, 8729-8736.	5.6	26
29	Polydopamine-embedded Cu _{2â~x} Se nanoparticles as a sensitive biosensing platform through the coupling of nanometal surface energy transfer and photo-induced electron transfer. Analyst, The, 2015, 140, 4121-4129.	3.5	25
30	Rapid detection of a dengue virus RNA sequence with single molecule sensitivity using tandem toehold-mediated displacement reactions. Chemical Communications, 2018, 54, 968-971.	4.1	25
31	Highly Sensitive Detection of miR-21 through Target-Activated Catalytic Hairpin Assembly of X-Shaped DNA Nanostructures. Analytical Chemistry, 2021, 93, 14545-14551.	6.5	25
32	Efficient visible-light photocatalytic heterojunctions formed by coupling plasmonic Cu _{2â^'x} Se and graphitic carbon nitride. New Journal of Chemistry, 2015, 39, 6186-6192.	2.8	24
33	Fluorescent quantification of terazosin hydrochloride content in human plasma and tablets using second-order calibration based on both parallel factor analysis and alternating penalty trilinear decomposition. Analytica Chimica Acta, 2009, 650, 143-149.	5.4	23
34	Graphitic C3N4 nanosheet and hemin/G-quadruplex DNAzyme-based label-free chemiluminescence aptasensing for biomarkers. Talanta, 2019, 192, 400-406.	5.5	23
35	Reduced graphene oxide coated Cu 2â~'x Se nanoparticles for targeted chemo-photothermal therapy. Journal of Photochemistry and Photobiology B: Biology, 2018, 180, 9-16.	3.8	22
36	Simultaneous determination of psoralen and isopsoralen in plasma and Chinese medicine Xian Ling Gu Bao capsule by using HPLC-DAD coupled with alternating trilinear decomposition algorithm. Analytica Chimica Acta, 2009, 650, 160-166.	5.4	21

#	Article	IF	CITATIONS
37	Tuning of the near-infrared localized surface plasmon resonance of Cu _{2â^'x} Se nanoparticles with lysozyme-induced selective aggregation. RSC Advances, 2014, 4, 55094-55099.	3.6	21
38	Identifying protein arginine methylation sites using global features of protein sequence coupled with support vector machine optimized by particle swarm optimization algorithm. Chemometrics and Intelligent Laboratory Systems, 2015, 146, 102-107.	3.5	20
39	Aggregation-induced superior peroxidase-like activity of Cu _{2â^'x} Se nanoparticles for melamine detection. Analytical Methods, 2016, 8, 7516-7521.	2.7	20
40	Highly selective detection of spermine in human urine via a nanometal surface energy transfer platform. Talanta, 2018, 188, 218-224.	5.5	20
41	Sensitive and selective turn off-on fluorescence detection of heparin based on the energy transfer platform using the BSA-stabilized Au nanoclusters/amino-functionalized graphene oxide hybrids. Talanta, 2016, 161, 482-488.	5.5	18
42	Simultaneous determination of metronidazole and tinidazole in plasma by using HPLC-DAD coupled with second-order calibration. Chinese Chemical Letters, 2010, 21, 1223-1226.	9.0	17
43	A visual physiological temperature sensor developed with gelatin-stabilized luminescent silver nanoclusters. Talanta, 2015, 143, 469-473.	5.5	17
44	The localized surface plasmon resonance induced edge effect of gold regular hexagonal nanoplates for reaction progress monitoring. Chemical Communications, 2018, 54, 13359-13362.	4.1	17
45	Discrimination of copper and silver ions based on the label-free quantum dots. Talanta, 2020, 220, 121430.	5.5	17
46	Aptamer-modified selenium nanoparticles for dark-field microscopy imaging of nucleolin. Chemical Communications, 2017, 53, 13047-13050.	4.1	16
47	Dopamine derived copper nanocrystals used as an efficient sensing, catalysis and antibacterial agent. RSC Advances, 2015, 5, 55832-55838.	3.6	15
48	Insight into a reversible energy transfer system. Nanoscale, 2016, 8, 16236-16242.	5.6	15
49	Large-scale preparation of fernwort-like single-crystalline superstructures of CuSe as Fenton-like catalysts for dye decolorization. Science China Chemistry, 2016, 59, 903-909.	8.2	15
50	A single gold nanoprobe for colorimetric detection of silver(<scp>i</scp>) ions with dark-field microscopy. Analyst, The, 2019, 144, 2011-2016.	3.5	15
51	Visual Identification of Light-Driven Breakage of the Silver-Dithiocarbamate Bond by Single Plasmonic Nanoprobes. Scientific Reports, 2015, 5, 15427.	3.3	14
52	Multiplex protein pattern unmixing using a non-linear variable-weighted support vector machine as optimized by a particle swarm optimization algorithm. Talanta, 2016, 147, 609-614.	5.5	14
53	Enzymeâ€ŧriggered fluorescence turnâ€off/turnâ€on of carbon dots for monitoring βâ€glucosidase and its inhibitor in living cells. Luminescence, 2020, 35, 222-230.	2.9	14
54	In situ investigating the size-dependent scattering signatures and sensing sensitivity of single silver nanocube through a multi-model approach. Journal of Colloid and Interface Science, 2021, 584, 253-262.	9.4	14

#	Article	IF	CITATIONS
55	Plasmonic biosensor for the highly sensitive detection of microRNA-21 via the chemical etching of gold nanorods under a dark-field microscope. Biosensors and Bioelectronics, 2022, 201, 113942.	10.1	13
56	Adaptive Configuring of Radial Basis Function Network by Hybrid Particle Swarm Algorithm for QSAR Studies of Organic Compounds. Journal of Chemical Information and Modeling, 2006, 46, 2494-2501.	5.4	12
57	Nonstoichiometric Cu _{2â^'x} Se nanocrystals in situ produced on the surface of carbon nanotubes for ablation of tumor cells. New Journal of Chemistry, 2016, 40, 6315-6324.	2.8	12
58	Resonance light scattering technique for sensitive detection of heparin using plasmonic Cu2-xSe nanoparticles. Talanta, 2020, 216, 120967.	5.5	12
59	Visual detection of cancer cells by using <i>in situ</i> grown functional Cu _{2â''x} Se/reduced graphene oxide hybrids acting as an efficient nanozyme. Analyst, The, 2019, 144, 716-721.	3.5	11
60	Dual-aptamer-based enzyme linked plasmonic assay for pathogenic bacteria detection. Colloids and Surfaces B: Biointerfaces, 2022, 214, 112471.	5.0	11
61	Automatic configuration of optimized sample-weighted least-squares support vector machine by particle swarm optimization for multivariate spectral analysis. Analytical Methods, 2010, 2, 282.	2.7	10
62	Vertically aligned gold nanomushrooms on graphene oxide sheets as multifunctional nanocomposites with enhanced catalytic, photothermal and SERS properties. RSC Advances, 2016, 6, 93645-93648.	3.6	10
63	Highly sensitive fluorescence quantification of irinotecan in biological fluids with the aid of second-order advantage. Chinese Chemical Letters, 2010, 21, 1482-1486.	9.0	9
64	Determination of benzo[a]pyrene in cigarette mainstream smoke by using mid-infrared spectroscopy associated with a novel chemometric algorithm. Analytica Chimica Acta, 2016, 902, 43-49.	5.4	9
65	Catalytic chemiluminescent detection of cholesterol in serum with Cu2â^'x Se semiconductor nanoparticles. Analytical and Bioanalytical Chemistry, 2016, 408, 8771-8778.	3.7	9
66	Nonstoichiometric copper chalcogenides for photo-activated alkyne/azide cycloaddition. Physical Chemistry Chemical Physics, 2017, 19, 6964-6968.	2.8	9
67	Modulation of inner filter effect between plasmonic Cu2â^'S Se1â^' and rhodamine 6G for detection of biothiols. Sensors and Actuators B: Chemical, 2018, 262, 966-973.	7.8	9
68	Rapid detection of heparin by gold nanorods and near-infrared fluorophore ensemble based platform via nanometal surface energy transfer. Sensors and Actuators B: Chemical, 2018, 274, 318-323.	7.8	9
69	Europium coordination polymer particles based electrospun nanofibrous film for point-of-care testing of copper (II) ions. Talanta, 2021, 228, 122270.	5.5	9
70	Long-distance transfer of plasmonic hot electrons across the Au–Pt porous interface for the hydrogen evolution reaction. Journal of Materials Chemistry C, 2021, 9, 3108-3114.	5.5	8
71	Lighting up of carbon dots for copper(<scp>ii</scp>) detection using an aggregation-induced enhanced strategy. Analyst, The, 2022, 147, 417-422.	3.5	8
72	Plasmonic locator with subâ€diffractionâ€limited resolution for continuously accurate positioning. Aggregate, 2022, 3, .	9.9	7

#	Article	IF	CITATIONS
73	Size-Dependent Plasmonic Resonance Scattering Characteristics of Gold Nanorods for Highly Sensitive Detection of microRNA-27a. ACS Applied Bio Materials, 2021, 4, 3469-3475.	4.6	6
74	A high-integrated DNA biocomputing platform for MicroRNA sensing in living cells. Biosensors and Bioelectronics, 2022, 207, 114183.	10.1	6
75	H ₂ S bubbles-assisted synthesis of hollow Cu _{2â^x} Se _y S _{1â^y} /reduced graphene oxide nanocomposites with tunable compositions and localized surface plasmon resonance. RSC Advances, 2015, 5, 91206-91212.	3.6	4
76	A label-free turn ON–OFF chemiluminescence strategy for lysozyme detection by target-triggered Cu _{2â^'x} Se aggregation. Analytical Methods, 2019, 11, 4376-4381.	2.7	4
77	Simultaneous Determination of Dextromethorphan and Quinidine Contents in Biological Fluid Samples Using Excitation-Emission Matrix Fluorescence Coupled with Second-Order Calibration Methods. Analytical Letters, 2010, 43, 2739-2750.	1.8	3
78	Glutathione-driven Cu(<scp>i</scp>)–O ₂ chemistry: a new light-up fluorescent assay for intracellular glutathione. Analyst, The, 2018, 143, 2486-2490.	3.5	3
79	The restructure of Au@Ag nanorods for cell imaging with dark-field microscope. Talanta, 2022, 244, 123403.	5.5	3
80	Yolkâ€5hell AuAgPt Alloy Nanostructures with Tunable Morphologies: Plasmonâ€Enhanced Photothermal and Catalytic Properties. Advanced Energy and Sustainability Research, 2022, 3, .	5.8	3
81	ZnO micron rods as single dielectric resonator for optical sensing. Analytica Chimica Acta, 2020, 1109, 107-113.	5.4	2
82	Gold triangular nanoplates with edge effect for reaction monitoring under dark-field microscopy. Colloids and Surfaces A: Physicochemical and Engineering Aspects, 2022, 647, 129133.	4.7	2
83	Fluorescence turn-on Cu2-xSe@HA-rhodamine 6G FRET nanoprobe for hyaluronidase detection and imaging. Journal of Photochemistry and Photobiology B: Biology, 2022, 233, 112496.	3.8	2